Improvement of the memory function by negative autoregulation of a mutual repression network in a stochastic environment

Short title: Stochastic memory in mutual repression networks improves by negative autoregulation

A B M Shamim Ul Hasan[1,2], Hiroyuki Kurata[2,*], Sebastian Pechmann[1,*]

[1] Department of Biochemistry, Université de Montréal, 2900 Edouard Montpetit Blvd, Montreal, QC, H3T 1J4, Canada

[2] The Biomedical Informatics R&D Center, Kyushu Institute of Technology, 680-4 Kawazu, Iizuka, Fukuoka 820-8502, Japan

* E-mail : kurata@bio.kyutech.ac.jp (HK); sebastian.pechmann@umontreal.ca (SP)

Abstract

Cellular memory is a ubiquitous function of biological systems. By generating a sustained response to a transient inductive stimulus, often due to bistability, memory is central to the robust control of many important biological functions. However, our understanding of the mechanistic basis of cellular memory remains incomplete. Specifically, stochastic fluctuations that are inherent to most biological systems have been shown to hamper memory function. Yet, how stochasticity changes the behavior of genetic circuits is generally not clear from a deterministic analysis of the network alone. Here, we apply deterministic, stochastic, and theoretical analyses to investigate how intrinsic noise affects the memory function in a mutual repression network. We find that the addition of negative autoregulation improves the persistence of memory by reducing stochastic fluctuations. Our theoretical analyses reveal that this improved memory function stems from an increased stability of the steady states of the system. Moreover, we show how the tuning of critical network parameters can further enhance memory. Our work highlights the power of stochastic and theoretical approaches to understanding biological circuits, and the importance of considering stochasticity to designing synthetic circuits with memory function.

Keywords: Memory, Mutual repression, Negative autoregulation, Fokker-Planck, Stochasticity, Hill coefficient, Bistability, Probability density

Introduction

Memory is ubiquitous in biological systems [1-4]. Characterized by a continued response to a transient stimulus [5], cellular memory has been found to aid in the robust control of divers biological functions such as synaptic plasticity [6], differentiation [7, 8], cell cycle transition [9], or gene regulation [10]. Memory in cellular circuitry is tightly linked to bistability, i.e. the presence of two stable steady states [11]. To this end, memory is achieved if an input signal evokes a switch to an alternative steady state where the system remains over time even after the input signal has disappeared [11].

Our general understanding of design principles of biological networks has improved dramatically during recent years [12]. Feedback loops as elementary components provide common control mechanisms of cellular networks [13]. For instance, negative feedback can facilitate adaptation and oscillation [14], while positive feedback loops, which play pivotal roles in cellular signaling [15], often promote signal amplification, bistable switches [16] and memory [11]. Indeed, a common circuit architecture that gives rise to memory is based on interlinked positive feedback network loops [17, 18]. Several experimental and theoretical analyses of such network architectures that can give rise to memory have been reported [7, 19, 20, 21, 24]. These studies have revealed many general properties underlying successful memory, for instance, that ultrasensitivity may be sufficient to generate two stable states [25], and that the transition periods between the bistable states compose an important characteristic of a cellular memory module [18]. In all cases, bistability and memory can use a transient input signal to yield a robust cellular system [26, 27]. This property is directly visible from the characteristic hysteresis behavior observed for bistability and memory systems. Experimental examples confirm these findings, such as the presence of hysteresis behavior and bistability in the budding yeast galactose-signaling networks [17]. Based on these general principles that link network architecture to systems behavior, the blossoming field of synthetic biology has contributed many useful designs of genetic circuits based on a rational understanding of biological networks [28-30] with myriad implications for biotechnology, biocomputing and gene therapy [12,25,31]. However, the rational design of robust memory function can be

implemented via many alternative mechanisms that remain incompletely understood and continues to be a very active field of research [20, 28].

Importantly, the vast majority of genes in a cell is normally only expressed at very low levels, thus giving rise to substantial stochastic fluctuations [32-38]. As a result, the analysis and design of biological circuits cannot be based solely on deterministic properties of the network topology alone. Instead, any interpretation has to take into consideration the functioning of a circuit architecture in a stochastic context. Accordingly, noise in gene regulatory networks has been found to fulfill important roles, for instance, during development or cellular fate determination [16, 39]. Similarly, extensive work has established general principles underlying the design of genetic circuits that exhibit bistability and memory [11, 40, 41, 42]. While an increasingly quantitative understanding of these circuits is emerging [7, 12, 19, 43], the effect of intrinsic noise is generally not taken into consideration. Recent examples of opposing behavior further highlight the importance of considering the contribution of stochasticity to cellular circuitry. On the one hand, it has been shown that noise can induce bistability and even stochastic memory in a system that, according to a deterministic description, lacks bistability [44]. On the other hand, stochastic fluctuations in gene expression levels often reduce or disrupt the memory function of biological networks [20, 45, 46]. To this end, the ability to sustain memory under noise is a key property of cellular systems [20]. However, to better understand the mechanistic basis of stochastic memory, the contributions of stochastic fluctuations have to be taken into account. Recent work highlights the power of computational and theoretical analyses to address exactly this need [47].

Here, we investigate how a negative autoregulation network architecture can improve the sustained memory function of a mutual repression network in a stochastic environment. Two types of gene regulatory networks, the regulated mutual repression network (MRN), and the regulated mutual repression network with negative autoregulation (MRN-NA) were investigated. Both networks are characterized by a mutual repression cycle that can give rise to bistability and memory. These network models were adopted from two well-characterized mutual repression networks, the system consisting of LacI and TetR in *E. coli* that displays a bistable gene expression memory module [23], and the mutual repression of the two repressors cI and Cro that

yield a bistable memory module in the bacteriophage λ [20]. In these cases, the mutual repression due to the positive feedback loop generates a memory function. However, a systematic analysis of the mechanisms underlying persistent memory in mutual repression networks remains lacking. To explore and compare the memory behavior between the MRN and MRN-NA network models, deterministic, stochastic and theoretical analyses were employed to identify principles of the robustness of the memory function. We demonstrate how negative autoregulation can reduce intrinsic noise and thus improve memory function by increasing the stability of the steady states. Systematic analyses of successful memory as function of central model parameters that describe the mutual repression cycle reveal the mechanistic basis and limits of memory function in mutual repression networks. By systematically evaluating two model systems under stochastic fluctuations, our results contribute important insights into the functioning of biological circuits in the presence of noise, and how they may be disrupted in pathological states. Moreover, our work highlights the importance of considering stochasticity when designing synthetic circuits with memory function.

Results

To investigate the effect of stochasticity on the memory function of mutual repression networks, we constructed two models of a gene regulatory network, shown in Figure 1 following a previously established graphical notation [48, 49]. The first model, the regulated mutual repression network (MRN) consists of proteins $y(1)$, $y(2)$ and $y(3)$ (Fig. 1A). An input signal S induces the synthesis of $y(1)$, which activates and represses the syntheses of $y(2)$ and $y(3)$, respectively. The syntheses of $y(2)$ and $y(3)$ are mutually repressed with cooperativity. The second model, the regulated mutual repression network model with negative autoregulation (MRN-NA), is a variant of the MRN model that introduces negative autoregulation to the $y(2)$ and $y(3)$ synthesis reactions (Fig. 1B). The addition of negative autoregulation permits to investigate how negative feedback loops may affect memory. In the following, we describe how the different architectures of the MRN-NA and the MRN gene regulatory networks alter the persistence of memory. To compare the memory regions of these two networks across our deterministic, stochastic, and theoretical analyses, the values of the corresponding kinetic parameters as well as the steady state levels of $y(2)$ and $y(3)$ were conserved as much as possible (Tables 1 and 2, Text S1 and S2).

The MRN model exhibits memory function

We first investigated the MRN model by deterministic and stochastic simulation. Herein, we analyzed the systems behavior at parameters previously identified to result in memory, namely Hill coefficients of $n = 7$ and $n = 8$ and dissociation constants of $K(2) = K(4) = 43$ (Table 3) [47]. The transient input signal S was applied between time steps 250 to 500, resulting, as expected, in S-induced $y(1)$, activation of $y(2)$ and suppression $y(3)$ (Fig. 2A).

The opposing dynamic behavior of $y(2)$ and $y(3)$ resulted directly from the network structure and choice of corresponding parameters that regulate $y(2)$ and $y(3)$ (Table 3) [47]. The initial conditions were set so that $y(2)$ occupies a low and $y(3)$ a higher

value. The input signal S evokes a switch-like response where $y(2)$ production increases and $y(3)$ levels are reduced. Importantly, proteins $y(2)$ and $y(3)$ showed a clear memory effect upon termination of the input signal S in our deterministic simulations. Even after S disappeared at time step 500, a high level of $y(2)$ and low level of $y(3)$ were sustained (Fig. 2A). This deterministic memory is the result of the mutual repression network architecture that yields a bistable system. An analysis of the corresponding hysteresis behavior supports this explanation for the observed memory (Fig. 2BC). Upon increasing S to sufficient signal strength, $y(2)$ production increased from a low to high level (Fig. 2B; dotted line). However, with a decrease in S the level of $y(2)$ stayed at a high level (Fig. 2B; solid line). Similarly, the $y(3)$ level decreased with an increase in S (Fig. 2C; dotted line), but increased sharply upon reduction of S (Fig. 2C; solid line). This hysteresis behavior is slightly more pronounced at higher Hill coefficient $n = 8$ compared to $n = 7$ and originated from the bistability generated by mutual repression. In general, this deterministic analysis suggested very similar dynamic behavior of the system for both Hill coefficients $n = 7$ and $n = 8$ with clear evidence of memory (Fig. 2A).

Next, we evaluated the same system in a stochastic environment (Fig. 2D,E). The stochastic dynamics of the MRN were simulated with the Gillespie method [52]. Strikingly, in a stochastic context the presence of memory was now found to depend on the strength of cooperativity in the mutual repression cycle. At lower Hill coefficient ($n = 7$), memory was not pertained and the values of $y(2)$ and $y(3)$ returned to their initial levels shortly after the loss of the input signal S (Fig. 2D). In contrast, at higher cooperativity ($n = 8$), successful memory was observed even in the context of intrinsic fluctuations of protein levels (Fig. 2E). It is well established that noise or a stochastic perturbation can flip gene expression levels from one to the other steady state [38]. Our results further demonstrated how stochasticity can deteriorate memory, as well as how increased cooperativity can confer increased robustness to memory function.

The MRN-NA model increases the robustness of memory

We next constructed the MRN-NA model to investigate the effect of negative autoregulation on memory function (Fig. 1B). For direct comparison, the steady state levels were set to the same values as in the MRN model (Text S3). Accordingly, we kept the dissociation constants $K(2) = K(4) = 43$ and probed the systems behavior at Hill coefficients of $n = 7$ and $n = 8$. The parameter values for $K(5)$ and $K(6)$, describing the negative autoregulation, were chosen to yield comparable behavior to the MRN model with all other parameters remaining unchanged (Table 3). Specifically, the model was parameterized such that the low and high steady state levels that could be assumed by $y(2)$ and $y(3)$ were almost the same in the MRN and MRN-NA networks.

As previously observed for MRN, the deterministic solution to the time evolution of the MRN-NA model showed clear memory after loss of the input signal S for both Hill coefficients of $n = 7$ and $n = 8$ (Fig. 3A). Similarly, strong hysteresis behavior was observed for both $y(2)$ and $y(3)$ levels as function of increasing and decreasing S (Fig. 3A,B). The addition of negative autoregulation, moreover, further reduced the small differences observed for $n = 7$ and $n = 8$ in the deterministic context. Remarkably, stochastic simulations of the MRN-NA model revealed strong and persistent memory both with Hill coefficients $n = 7$ (Fig. 3D) and $n = 8$ (Fig. 3E). Importantly, the MRN alone could not sustain memory for either $y(2)$ or $y(3)$ at $n = 7$ in a stochastic context (Fig. 2D), but the MRN-NA yielded strong and sustained memory due to the addition of negative feedback loops (Fig. 3D). We further verified that the addition of negative autoregulation hardly affected the dynamics of the MRN (Figs. 2 and 3).

To further understand how the addition of negative autoregulation increases the robustness of the memory function, we sought to quantify the intrinsic noise in the protein levels of $y(2)$ and $y(3)$ in the MRN and MRN-NA models. To obtain a reliable and comparable estimate, we computed the coefficients of variation (CVs) during active signal S when the models are parameterized to yield the same values of $y(2)$ and $y(3)$. The interval from time steps 270 to 480 was chosen to allow the

system to respond to the stimulus for 20 times steps on either end of the signal period. Our analysis of noise in protein levels $y(2)$ and $y(3)$ as function of the dissociation constants $K(2) = K(4)$ that describe the mutual repression in the network confirmed a systematic reduction of stochasticity in $y(2)$ and $y(3)$ levels upon the addition of negative autoregulation (Fig. 3F). While maintaining the same steady state levels, noise was dramatically reduced for $y(3)$ (Fig. 3F). Of note, by populating the lower steady state $y(3)$ is more susceptible to noise. Similarly, intrinsic fluctuations in $y(2)$ during the signal period were reduced in the MRN-NA compared to the MRN model in our stochastic simulations irrespective of the dissociation constants tested (Fig. 3F). Taken together, our results suggest that the negative autoregulation played a vital role in generating stochastic memory by reducing intrinsic noise.

Memory regions of the MRN and MRN-NA models

Our analyses so far have established that both the MRN and the MRN-NA models can exhibit memory, which however critically depends on persistent mutual repression with strong cooperativity. To establish more generally the memory function of these networks and further explore their ability to display memory function outside the specific parameter sets discussed so far, we set out to systematically map their memory region as function of Hill coefficient and dissociation constants $K(2) = K(4)$ (Fig. 4). Successful memory was defined as sustained levels of $y(2)$ and $y(3)$ at or near their levels during the applied *S* after the end of the input signal *S* at time step 500 until the end of the simulations at time step 1000. Moreover, for most direct comparison, the kinetic parameter $k(7)$ was adjusted to conserve the steady-state levels among the two models as much as possible (Table 2; Text S1 and S2). Memory was assessed in both the deterministic and stochastic context (see Methods). Accordingly, two memory regions were defined: deterministic memory (Fig. 4**;** both cyan and red areas), and stochastic memory (Fig. 4; only red areas). Outside these areas, the models were either not bistable or could not sustain memory (Fig. 4).

In both the MRN and MRN-NA models, deterministic memory could be observed for Hill coefficients of $n = 4$ or greater (Fig. 4). In contrast, stochastic memory not only generally required higher Hill coefficients, but also posed different limits on the MRN and MRN-NA models. Without negative autoregulation that suppresses noise, stochastic memory in the MRN model required a Hill coefficient of $n = 8$ or greater (Fig. 4A). In the presence of negative autoregulation that reduces noise in protein levels, stochastic memory in the MRN-NA model could be observed already from $n = 7$ (Fig. 4B). Thus, the MRN required a higher level of cooperativity to generate stochastic memory.

Generally, the stochastic memory region for the MRN-NA model was found to be larger than for the MRN model (Fig. 4, red areas), indicating that negative autoregulation of the MRN-NA enhances memory function by reducing intrinsic noise. While the deterministic memory regions in both networks are essentially the same (Fig. 4, cyan areas), it was clearly more difficult to maintain a memory effect under noise in the MRN than the MRN-NA (Fig. 4; red areas). The large areas that only permit deterministic memory indicate the general challenge of maintaining memory function in the context of stochasticity.

Stochastic potential of the MRN and MRN-NA models

Prerequisite for memory is normally the presence of bistability in the system. Thus, a limited bistable regime could explain why such high levels of strength and cooperativity in the mutual repression between $y(2)$ and $y(3)$ were required to yield memory. To map out the bistable regimes of the MRN and MRN-NA models, theoretical analyses based on the chemical master equations were employed to support the numerical simulation results.

First, the corresponding Fokker-Planck equations (Eq. (11)) describing the time evolution of the probability densities for $y(2)$ and $y(3)$ levels were derived from the six rate equations (Eqs. (1-6)). We validated that the solutions to the Fokker-Planck equations were consistent with the probability densities obtained by stochastic simulation (Text S5). By using the Fokker-Planck equations, we next estimated the

two-dimensional stochastic bistable regions for the MRN and MRN-NA models as function of the Hill coefficient and dissociation constants (Fig. 5, Text S1, S2 and S6).

In these theoretical analyses, both the MRN and the MRN-NA models permitted bistability starting from a Hill coefficient of $n = 3$ for both $y(2)$ and $y(3)$ (Fig. 5). However, the bistable regions in the MRN-NA were clearly larger than in the MRN model (Fig. 5). To display bistability in a stochastic context, the MRN model required dissociation constants $K(2) = K(4)$ within a more constrained parameter space (Fig. 5). These analyses established that the MRN-NA more readily exhibits stochastic bistability than the MRN. Conversely, a more limited bistability regime in the MRN in a stochastic context (Fig. 5) contributes to explaining why this network had a smaller stochastic memory region (Fig. 4).

Mean first-passage time of the MRN and MRN-NA models

Having established that the presence of memory in the MRN and MRN-NA models depended on both bistability and robustness of the steady states to stochasticity, we next sought to further explore the origins and limits of memory functionality in context of fluctuating protein levels. To this end, the stability of a steady state of a stochastic system can be estimated by the mean first-passage time (MFPT). The MFPT quantifies the average number of time steps it takes for a system to leave a favorable steady state due to random events. As such, the MFPT provides a useful description of the time-scale on which a phase transition is likely to happen [56, 58]. Thus, because the presence of a stochastic bistable region only indicates the bimodality of gene expression as prerequisite for memory but not the presence of memory itself, a MFPT analysis can be helpful for identifying the precise conditions under which memory can be attained in a stochastic context.

Here, MFPT analyses were performed between the two stable steady states (see Methods). Specifically, we calculated the MFPTs of $y(2)$ and $y(3)$ for both the MRN and MRN-NA models (Fig. 6); the low and high steady-states of $y(2)$ and $y(3)$ are

denoted as $y(2)_l^{st}, y(2)_u^{st}$, $y(3)_l^{st}$ and $y(3)_u^{st}$, respectively. Accordingly, the MFPTs of leaving the lower (T_L) and upper (T_U) steady states were calculated as function of the Hill coefficient and dissociation constants in the mutual repression cycle for $y(2)$ and $y(3)$.

Due to the asymmetry in the MRN and MRN-NA models (Table 2, 3), the MFPTs for $y(2)$ and $y(3)$ showed opposing behavior, as expected (Fig. 6): while the MFPT for $y(2)$ to leave the lower steady state, $T_L(y(2)_l^{st})$, is consistently higher than the corresponding time to leave the upper steady state, $T_U(y(2)_u^{st})$, the system is in generally much more likely to leave the lower steady state of $y(3)$ as indicated by $T_L(y(3)_l^{st})$ being much smaller than $T_U(y(3)_u^{st})$ (Fig. 6).

An increase of the Hill coefficient as measure of cooperativity exacerbated this trend observed for the MFPTs of $y(2)$ and $y(3)$ (Fig. 6A). The prolonged MFPTs as a result of increasing Hill coefficients explained for both models why the robustness of sustaining stochastic memory improved with increasing cooperativity. In general, stability of the high steady state is more persistent in both models independent of the Hill coefficient, as evident by $T_L(y(2)_l^{st}) > T_U(y(2)_u^{st})$ (Fig. 6A). Moreover, all MFPTs for the MRN-NA, $T_L(y(2)_l^{st})$, $T_U(y(2)_u^{st})$, $T_L(y(3)_l^{st})$, and $T_U(y(3)_u^{st})$, were observed to be longer than their equivalents for the MRN model, also independent of the Hill coefficient (Fig. 6A). These results confirm an increased stability of the steady states upon introduction of negative autoregulation in MRN-NA compared to MRN, which explains the improved memory function in the MRN-NA system.

Similarly, we investigated the effect of the dissociation constants in the mutual repression cycle on the MFPTs of $y(2)$ and $y(3)$ (Fig. 6B). Consistently, the MFPTs for all steady states, $T_L(y(2)_l^{st})$, $T_L(y(3)_l^{st})$, $T_U(y(2)_u^{st})$ and $T_U(y(3)_u^{st})$, were found to be longer in the MRN-NA compared to the MRN independent of the dissociation constants (Fig. 6B). This result further underlines how the MRN-NA could realize more persistent memory than the MRN. In other words, the MRN

memory is more fragile than that in the MRN-NA. For both the models, all MFPTs, $T_L(y(2)_l^{st})$, $T_U(y(2)_u^{st})$, $T_L(y(3)_l^{st})$ and $T_U(y(3)_u^{st})$ gradually decreased with an increase in the dissociation constant. This analysis suggests that strong binding in the mutual repression cycle is necessary for persistent memory. In summary, these MFPT analyses illuminated in detail how memory in the mutual repression networks improved with increasing robustness of the steady states as function of higher cooperativity strength in the mutual repression cycle.

Probability densities of the steady-state levels in MRN and MRN-NA

The previous analyses revealed a strong dependency of sustained memory on the robustness of the steady-states. To formally establish the probability densities associated with populating the upper and lower steady states of $y(2)$ and $y(3)$, we calculated the probability densities from the Fokker-Planck Equations (Eq. (18)) for the MRN and MRN-NA models as function of the Hill coefficient and dissociation constants (Fig. 7). The probability density of the high steady state of $y(2)$ increased while that of the corresponding lower steady state decreased with an increase in the Hill coefficient for both the MRN and the MRN-NA models (Fig. 7A). The addition of negative autoregulation in the MRN-NA system visibly made the upper steady state level of $y(2)$ more dominant (Fig. 7A).

The probability density associated to $y(3)$ more clearly illustrated the evolution of bistability and subsequent increased robustness of the steady states with increasing Hill coefficient (Fig. 7B). At low Hill coefficient $(n = 3)$ the MRN lacked a pronounced probability density associated with a lower steady state (Fig. 7B, solid blue line) while in the MRN-NA the probability density did not separate well the peaks at lower and higher levels of $y(3)$ (Fig. 7B, dashed blue line). This result of weak bistability was consistent with our previous analysis of the bistability regions (Fig. 5). In turn, higher Hill coefficients of $n = 8$ and $n = 12$ promoted first the emergence and then separation of two clearly populated steady states (Fig. 7B). While the higher steady state of $y(3)$ was dominant at $n = 8$, at $n = 12$ the system switched to a dominant lower steady state for $y(3)$ (Fig. 7B). Moreover, the addition of negative autoregulation strongly promoted the population of the lower steady state at

all Hill coefficients analyzed (Fig. 7B, dashed lines). By buffering intrinsic noise, this analysis thus confirmed that the negative feedback loops stabilized particularly the low expression states of $y(3)$, i.e. those that are most susceptible to fluctuations.

Similarly, the probability densities of $y(2)$ and $y(3)$ were found to quantitatively and qualitatively also depend on the dissociation constants $K(2)$ and $K(4)$ in the mutual repression cycle (Fig. 7C,D). At low $K(2) = K(4) = 15$, the low and high steady states of $y(2)$ were about equally probable in the MRN, while the high steady state remained dominant in the MRN-NA model (Fig. 7C). With increasing values of $K(2)$ and $K(4)$ the lower steady state became more pronounced in both models, but even more so in the MRN (Fig. 7C). In contrast, the probability densities associated to $y(3)$ only change minimally with increasing dissociation constants. Herein, lower values for $K(2)$ and $K(4)$ as well as negative autoregulation favored more pronounced bistability (Fig. 7D). Taken together, these results established the theoretical basis for our observation that the MRN-NA model displays an improved memory function in a stochastic context.

Discussion

By applying deterministic, stochastic, and theoretical approaches, we here investigated the mechanism by which negative autoregulation can improve the memory function in a mutual repression network. Previous work had established the regulated mutual activation network (MAN) and mutual repression network (MRN) as good model systems to study fundamental properties of cellular memory as encoded in genetic circuitry [47]. However, a systematic analysis of the determinants and limits of sustained memory had not been performed [47]. Here, we aimed to systematically decouple contributions of negative autoregulation, as well as strength of cooperativity and dissociation constants in the mutual repression cycle to the persistence of memory function.

Stochasticity decreased the memory in both models. In particular, the stochastic memory of the MRN was very sensitive to the presence of noise at Hill coefficient $n = 7$ (Fig. 2D). In contrast, the MRN-NA achieved robust, persistent memory in both the deterministic and stochastic approaches even at a lower cooperativity $n = 7$ compared to the MRN (Fig. 3D). These results revealed that the MRN required a higher level of ultrasensitivity or cooperativity to sustain memory. The robustness of stochastic memory of the MRN-NA could be further improved by increasing the binding strength of the repressor proteins (Fig. 6B). Mapping out the memory regions with respect to a Hill coefficient and dissociation constants revealed that the MRN-NA model exhibited a more robust and larger memory area than the MRN in noisy cellular environments (Fig. 4A, B). Because noise is omnipresent in genetic networks, we examined the mechanisms by which the memory region of the MRN is altered through noise-reducing negative autoregulation. By comparing the MRN and MRN-NA models, we demonstrated that negative feedback loops are effective at reducing noise, thus enhancing the robustness of memory (Fig. 3F and Fig. 4).

To gain more general insights into the determinants of successful memory, systematic analyses of the dependence of sustained memory and bistability on Hill coefficient and dissociation constants in the mutual repression cycle were performed to generate phase diagrams for the bistability as well as deterministic and stochastic memory regions (Fig. 4, 5). The results not only revealed mechanistic insights into the sensitivity of memory function to noise but also highlighted the need for biological parameters to be finely tuned to achieve robust memory. Indeed, only a small part of the possible parameter space yielded sustained memory.

To this end, while accurately simulating the time evolution of protein concentrations in stochastic systems, the Gillespie algorithm showed limited power in characterizing sustained memory due to its known computational cost. Many time-consuming simulations are required to determine reliably if a model exhibits persistent stochastic memory or not. Theoretical analyses can overcome this computational complexity. Here, two types of theoretical analyses were performed: MFPT analyses revealed insights into the stability of steady states. Moreover, calculations of the probability

densities revealed their separation and relative population of the steady states, thus even more directly informing on the robustness of memory. Because the presence of bistability alone is not sufficient for inferring sustained memory function, the theoretical MFPT analyses were able to make a distinct contribution. Specifically, the MFPT analysis indicated that the persistent stochastic memory achieved by the MRN-NA was more robust and stable than that achieved by the MRN, because the MFPTs of the low and high steady-states of $y(2)$ and $y(3)$ in the MRN-NA were clearly longer than those of the MRN. This finding supported our simulation results suggesting that the stochastic memory region of the MRN is very limited. In addition, the presented findings revealed the mechanism by which the cooperativity and binding strength of the repressors affect the stochastic memory of the MRN and MRN-NA. For both models, high cooperativity and low dissociation constants – or a corresponding increase in binding strength - extended the MFPT, thus sustaining the memory function. Taken together, our analyses systematically revealed the determinants for the successful generation of cellular memory in a stochastic environment.

In the present work, defined and validated sets of kinetic parameters were used instead of exhaustive searches for alternative parameter combinations that also give rise to memory. To generalize our findings, phase diagrams of the memory region were derived as function of the two most critical and previously identified parameters [47]. By doing so, we were able to reveal fundamental insights into the mechanisms underlying robust stochastic memory. Future work will expand how greater variability in parameter choices, for instance reflecting additional external cellular regulation of constituent genes, may allow to sustain stochastic memory. A second direction for further work will target systems of increased complexity as often found in biology. Efficient algorithms such as the tau-leap method [50] would keep this tractable. Known biological examples readily hint at such increased complexity that awaits to be further studied. For instance, a Notch-Delta mutual repression network serves to communicate between neighboring cells [51] where an increase in Notch activity within a cell decreases that in its neighboring cell. The Notch-Delta mutual repression provides inhomogeneous or opposite protein synthesis in homogeneous cell populations. To capture this phenomenon would require to consider spatial changes in

gene expression, which could be implemented as extension of both the MRN and MRN-NA models.

Last, our work makes direct predictions for the optimal design of memory in synthetic biology. Depending on the specific requirements, stochastic memory can be obtained by a simple MRN design. The addition of negative autoregulation comes at the cost of increased model complexity but clearly improves the robustness of the memory function in a stochastic context. Moreover, the memory of the MRN-NA model is also more robust to changes in kinetic parameters.

In summary, we have shown that the addition of negative autoregulation can reduce intrinsic noise and generate persistent stochastic memory. Our mathematical comparison and theoretical analysis of the two networks contributes to an improved understanding of how genetic circuits can encode biological function and may aid the rational engineering of memory networks for applications in synthetic biology, medicine and biotechnology.

Methods

Code availability

The computer code used to perform all analyses is available at https://github.com/ABMSUH/MRN-and-MRN-NA-models

MRN and MRN-NA models

We constructed two simple models of a gene regulatory network that consists of two genes encoding a transcription factor that we visualized according to the graphical notation [48, 49] (Fig. 1). The regulated mutual repression network (MRN) consists of proteins $y(1)$, $y(2)$ and $y(3)$ (Fig. 1A). The input signal S induces the synthesis of $y(1)$, which in turn activates the synthesis of $y(2)$ and represses production of $y(3)$. Furthermore, the synthesis reactions of both of $y(2)$ and $y(3)$ are mutually repressed with cooperativity. This system can be bistable and exhibit memory. The model is described by the following equations (1-3):

$$\frac{dy(1)}{dt} = k(1).S - k(2).y(1) \tag{1}$$

$$\frac{dy(2)}{dt} = k(3).\frac{y(1)}{y(1)+K(1)} + k(4).\frac{K(2)^n}{y(3)^n + K(2)^n} - k(5).y(2) \tag{2}$$

$$\frac{dy(3)}{dt} = k(6).\frac{K(3)}{y(1)+K(3)} + k(7).\frac{K(4)^n}{y(2)^n + K(4)^n} - k(8).y(3) \tag{3}$$

The mutual repression network with negative autoregulation (MRN-NA) is an extension of the MRN model where negative autoregulation was added to the $y(2)$ and $y(3)$ synthesis reactions to investigate how these negative feedback loops can affect the memory function of the system (Fig. 1B). The model is described by the following equations (4-6):

$$\frac{dy(1)}{dt} = k(1).S - k(2).y(1) \tag{4}$$

$$\frac{dy(2)}{dt} = k(3).\frac{y(1)}{y(1)+K(1)} + k(4).\frac{K(2)^n}{y(3)^n + K(2)^n}$$

$$+ k(9).\frac{K(5)}{y(2)+K(5)} - k(5).y(2) \qquad (5)$$

$$\frac{dy(3)}{dt} = k(6).\frac{K(3)}{y(1)+K(3)} + k(7).\frac{K(4)^n}{y(2)^n + K(4)^n}$$

$$+ k(10).\frac{K(6)}{y(3)+K(6)} - k(8).y(3) \qquad (6)$$

All parameters for both models are described in Table 1.

Systems modeling and determination of successful memory

The time evolution of the gene expression levels of $y(1)$, $y(2)$ and $y(3)$ in the MRN and MRN-NA models were simulated both deterministically and stochastically. For a deterministic systems description, the ordinary differential equations (Eqs. 1-6) were solved in MATLAB (Mathworks) with standard solvers. Stochastic trajectories were simulated with the Gillespie algorithm [52].

In all model simulations, the deterministic and stochastic time courses of $y(1)$, $y(2)$ and $y(3)$ were simulated for 1,000 time steps. The input signal *S* was applied from time step 250 to 500. Deterministic memory was defined as sustained protein levels in the deterministic simulations during the subsequent period from time steps 500 to 1000 after loss of the signal *S*. Similarly, stochastic memory was assessed as sustained protein levels in the stochastic simulations in the period from time steps 500 to 1000 after loss of the signal *S*. Due to the probabilistic nature of the stochastic simulations, robust stochastic memory for a given set of parameters was defined as successful if 18 out of 20 stochastic simulations, i.e. 90%, yielded persistent memory [47].

Theoretical comparison of the MRN and MRN-NA models

All parameters were set as to render the MRN and MRN-NA models as comparable as possible (Tables 1–3) [47, 53]. With the exception of the additional negative autoregulation loops, this meant using the same parameters throughout. The parameters of the negative autocorrelation were tuned to conserve the steady state levels of $y(2)$ and $y(3)$ between the MRN and MRN-NA models as much as possible (Tables 1–3). Given the asymmetry of the models (activation of $y(2)$ and suppression of $y(3)$ by S), the deterministic steady-state levels of $y(2)$ and $y(3)$ always show opposing behavior: when the steady-state level of $y(2)$ is high, that of $y(3)$ is low and vice versa. Our parameters choices conserved both the low and high steady states of $y(2)$ and $y(3)$ between the MRN and MRN-NA models (Text S1 and S2)

To systematically identify parameter choices that can give rise to successful memory, phase diagrams of the memory region as function of the two most critical parameters, the Hill coefficient and dissociation constants in the mutual repression cycle, were computed by successive simulation at different parameter combinations.

Intrinsic noise in gene expression was quantified by computing the coefficient of variation (CV) of the levels of $y(2)$ and $y(3)$ during the input signal S from the stochastic simulations. To eliminate transition effects, we considered the period from time steps 270 to 480, i.e. omitting 20 time steps on either end of the signal period.

Stochastic potential and probability density function

To theoretically perform deterministic and stochastic potential analysis, we converted the reaction rate equations (Eqs. 1-3) into the one-variable rate equations $f_{MRN2}(y)$ and $f_{MRN3}(y)$ by the quasi-steady-state approximation (Text S3). In the same manner, the reaction rate equations (Eqs. 4-6) were converted into $f_{MRN-NA2}(y)$ and

$f_{MRN-NA3}(y)$ (Text S4). Here, we illustrated how a one-variable equation $f_{MRN2}(y)$ is given under a stochastic environment by:

$$\frac{dy}{dt} = f_{MRN2}(y)$$
$$= k(4).\frac{K(2)^n}{[\{k(6).\frac{K(2)^n}{y^n + K(2)^n}\}.\frac{1}{k(8)}]^n + K(2)^n} - k(5).y \quad (7)$$

This equation can be described by the birth-and-death stochastic processes [20, 47, 54]:

$$W_{birth}(y) = k(4).\frac{K(2)^n}{[\{k(6).\frac{K(2)^n}{y^n + K(2)^n}\}.\frac{1}{k(8)}]^n + K(2)^n} \quad (8)$$

$$W_{death}(y) = k(5).y \quad (9)$$

The corresponding chemical master equation was given by:

$$\frac{\partial P(y,t)}{\partial t} = W_{birth}(y-1)P(y-1,t) + W_{death}(y+1)P(y+1,t) - \{W_{birth}(y) + W_{death}(y)\}P(y,t) \quad (10)$$

where $P(y,t)$ was the probability density of protein concentration *y*. Next, the chemical master equation was transformed into the Fokker-Planck equation [20, 47, 54-56]:

$$\frac{\partial P(y,t)}{\partial t} = -\frac{\partial}{\partial y}[A(y)P(y,t)] + \frac{1}{2}\frac{\partial^2}{\partial y^2}[B(y)P(y,t)] \quad (11)$$

where $$A(y) = k(4).\frac{K(2)^n}{[\{k(6).\frac{K(2)^n}{y^n + K(2)^n}\}.\frac{1}{k(8)}]^n + K(2)^n} - k(5).y \quad (12)$$

The noise function is given by:

$$B(y) = k(4).\frac{K(2)^n}{[\{k(6).\frac{K(2)^n}{y^n + K(2)^n}\}.\frac{1}{k(8)}]^n + K(2)^n} + k(5).y \quad (13)$$

In the same manner, the Fokker-Planck equations of the four one-variable equations including $f_{MRN2}(y)$ were solved under the following conditions (Text S3 and S4):

$$A(y) = \begin{cases} f_{MRN2}(y) & \text{for } y=y(2) \\ f_{MRN3}(y) & \text{for } y=y(3) \end{cases} \quad \text{for the MRN model} \qquad (14)$$

$$A(y) = \begin{cases} f_{MRN-NA2}(y) & \text{for } y=y(2) \\ f_{MRN-NA3}(y) & \text{for } y=y(3) \end{cases} \quad \text{for the MRN-NA model} \qquad (15)$$

and the noise functions were given by:

$$B(y) = \begin{cases} g_{MRN2}(y) & \text{for } y=y(2) \\ g_{MRN3}(y) & \text{for } y=y(3) \end{cases} \quad \text{for the MRN model} \qquad (16)$$

$$B(y) = \begin{cases} g_{MRN-NA2}(y) & \text{for } y=y(2) \\ g_{MRN-NA3}(y) & \text{for } y=y(3) \end{cases} \quad \text{for the MRN-NA model} \qquad (17)$$

Finally, we consider the stochastic potential analysis. The limit of $P(y,t)$ as $t \to \infty$ yields $P_{st}(y)$, the stationary probability density function of y [20, 47, 54], which is given by:

$$P_{st}(y) = \frac{N_c}{B(y)} \exp[2\int^{x} \frac{A(z)}{B(z)} dz]$$

(18)

where N_c is the normalization constant. Eq. (18) can be recast in the form:

$$P_{st}(y) = N_c e^{-2\Phi_S(y)}$$

(19)

where

$$\Phi_s(y) = \frac{1}{2}\ln[B(y)] - \int^{y} \frac{A(z)dz}{B(z)}$$

(20)

is called the stochastic potential of $f(y)$ [54, 56, 57].

Mean first-passage time analysis

In gene expression, the robustness or stability of a steady state has to be estimated in the presence of noise. The stability of a steady state of a stochastic system can be

estimated by the mean first-passage time (MFPT), which describes the expected time within which the system leaves a stable steady state due to random fluctuations. An equilibrium point can exit from its minimum potential due to the effect of noise. The exit time depends on the specific realization of the random process; this is known as the first passage time. The MFPT is the average of the first passage times over many realizations. In the context of anticipating phase shifts, the MFPT provides a useful tool to characterize the time-scale on which a phase transition is likely to occur.

Let us consider y_l^{st} and y_u^{st} ($y_l^{st} < y_u^{st}$) as two steady states corresponding to a low and a high protein concentration, respectively, separated by the unstable steady state defining the potential barrier y_b^{un} (i.e., the unstable equilibrium point). The basin of attraction of the state y_u^{st} extends from y_b^{un} to $+\infty$, as it is to the right of y_l^{st}. Let $T(y)$ be the MFPT to state y_b^{un} starting at $y > y_b^{un}$. $T(y)$ satisfies the following ordinary differential equation [20, 56, 58, 59]:

$$A(y)\frac{\partial T(y)}{\partial y} + \frac{1}{2}B(y)\frac{\partial^2 T(y)}{\partial y^2} = -1 \qquad (21)$$

with boundary conditions:

$$T(y_b^{un}) = 0 \text{ and } \frac{\partial T(+\infty)}{\partial y} = 0 \qquad (22)$$

By solving Eqs. (21-22), the MFPTs of y_u^{st} and y_l^{st} : $T_U(y_u^{st})$ and $T_L(y_l^{st})$ are calculated to state y_b^{un} for the basin of attraction of the state y_u^{st} extending from y_b^{un} to $+\infty$ and for the basin of attraction of the state y_l^{st} which extends from 0 to y_b^{un}, respectively, as follows:

$$T_L(y_l^{st}) = 2\int_{y_l^{st}}^{y_b^{un}} \frac{1}{\Psi(x)}dx.\int_0^x \frac{\Psi(z)}{B(z)}dz \qquad (23)$$

$$T_U(y_u^{st}) = 2\int_{y_b^{un}}^{y_u^{st}} \frac{1}{\Psi(x)}dx.\int_x^{\infty}\frac{\Psi(z)}{B(z)}dz \tag{24}$$

where

$$\Psi(y) = \exp(\int_{y_0}^{y} \frac{2A(w)}{B(w)}dw) \tag{25}$$

with $y_0 = 0$ for the $y_u^{st} \rightarrow y_l^{st}$ transition and $y_0 = y_b^{un}$ for the $y_l^{st} \rightarrow y_u^{st}$ transition.

A high value of the MFPT of a steady state protein level indicates that the level is sustained for a longer time, whereas a low value indicates that the protein can readily leave the steady state and quickly transition to another level.

Acknowledgments

We are grateful to Dr. Kazuhiro Maeda for helpful discussions. SP holds the Canada Research Chair in Computational Systems Biology and acknowledges funding from the Merck Sharp Dohme program of the Faculty of Medicine of the Université de Montréal.

Author Contributions

Conceptualized the research: ABMSUH, HK; Developed all methodology and performed all analysis: ABMSUH; Interpreted the results: ABMSUH, HK, SP; Wrote the original draft: ABMSUH; Reviewed and edited the final manuscript: ABMSUH, HK, SP.

References

1. Kandel ER, Dudai Y, Mayford MR. The molecular and systems biology of memory. Cell. 2014;157(1):163-86. Epub 2014/04/01. doi: 10.1016/j.cell.2014.03.001. PubMed PMID: 24679534.
2. Casadesus J, D'Ari R. Memory in bacteria and phage. BioEssays : news and reviews in molecular, cellular and developmental biology. 2002;24(6):512-8. doi: 10.1002/bies.10102. PubMed PMID: 12111734.
3. Harvey ZH, Chen Y, Jarosz DF. Protein-Based Inheritance: Epigenetics beyond the Chromosome. Molecular cell. 2018;69(2):195-202. Epub 2017/11/21. doi: 10.1016/j.molcel.2017.10.030. PubMed PMID: 29153393; PubMed Central PMCID: PMCPMC5775936.
4. Bergeron-Sandoval LP, Safaee N, Michnick SW. Mechanisms and Consequences of Macromolecular Phase Separation. Cell. 2016;165(5):1067-79. Epub 2016/05/21. doi: 10.1016/j.cell.2016.05.026. PubMed PMID: 27203111.
5. Burrill DR, Silver PA. Making cellular memories. Cell. 2010;140(1):13-8. doi: 10.1016/j.cell.2009.12.034. PubMed PMID: 20085698; PubMed Central PMCID: PMC2882105.
6. Shen K, Teruel MN, Connor JH, Shenolikar S, Meyer T. Molecular memory by reversible translocation of calcium/calmodulin-dependent protein kinase II. Nat Neurosci. 2000;3(9):881-6. Epub 2000/08/31. doi: 10.1038/78783. PubMed PMID: 10966618.
7. Xiong W, Ferrell JE, Jr. A positive-feedback-based bistable 'memory module' that governs a cell fate decision. Nature. 2003;426(6965):460-5. doi: 10.1038/nature02089. PubMed PMID: 14647386.
8. Wang L, Walker BL, Iannaccone S, Bhatt D, Kennedy PJ, Tse WT. Bistable switches control memory and plasticity in cellular differentiation. Proceedings of the National Academy of Sciences of the United States of America. 2009;106(16):6638-43. Epub 2009/04/16. doi: 10.1073/pnas.0806137106. PubMed PMID: 19366677; PubMed Central PMCID: PMCPMC2672527.

9. Doncic A, Atay O, Valk E, Grande A, Bush A, Vasen G, et al. Compartmentalization of a bistable switch enables memory to cross a feedback-driven transition. Cell. 2015;160(6):1182-95. Epub 2015/03/15. doi: 10.1016/j.cell.2015.02.032. PubMed PMID: 25768911; PubMed Central PMCID: PMCPMC4377233.
10. Herrera-Delgado E, Perez-Carrasco R, Briscoe J, Sollich P. Memory functions reveal structural properties of gene regulatory networks. PLoS computational biology. 2018;14(2):e1006003. Epub 2018/02/23. doi: 10.1371/journal.pcbi.1006003. PubMed PMID: 29470492.
11. Ajo-Franklin CM, Drubin DA, Eskin JA, Gee EP, Landgraf D, Phillips I, et al. Rational design of memory in eukaryotic cells. Genes & development. 2007;21(18):2271-6. doi: 10.1101/gad.1586107. PubMed PMID: 17875664; PubMed Central PMCID: PMC1973140.
12. Alon U. Network motifs: theory and experimental approaches. Nature reviews Genetics. 2007;8(6):450-61. doi: 10.1038/nrg2102. PubMed PMID: 17510665.
13. Brandman O, Meyer T. Feedback loops shape cellular signals in space and time. Science. 2008;322(5900):390-5. doi: 10.1126/science.1160617. PubMed PMID: 18927383; PubMed Central PMCID: PMC2680159.
14. Elowitz MB, Leibler S. A synthetic oscillatory network of transcriptional regulators. Nature. 2000;403(6767):335-8. doi: 10.1038/35002125. PubMed PMID: 10659856.
15. Freeman M. Feedback control of intercellular signalling in development. Nature. 2000;408(6810):313-9. doi: 10.1038/35042500. PubMed PMID: 11099031.
16. Hasty J, Pradines J, Dolnik M, Collins JJ. Noise-based switches and amplifiers for gene expression. Proceedings of the National Academy of Sciences of the United States of America. 2000;97(5):2075-80. doi: 10.1073/pnas.040411297. PubMed PMID: 10681449; PubMed Central PMCID: PMC15756.
17. Chang DE, Leung S, Atkinson MR, Reifler A, Forger D, Ninfa AJ. Building biological memory by linking positive feedback loops. Proceedings of the National Academy of Sciences of the United States of America. 2010;107(1):175-80. Epub 2009/12/19. doi: 10.1073/pnas.0908314107. PubMed PMID: 20018658; PubMed Central PMCID: PMCPMC2806707.

18. Ferrell JE, Jr. Self-perpetuating states in signal transduction: positive feedback, double-negative feedback and bistability. Current opinion in cell biology. [1]2002;14(2):140-8. PubMed PMID: 11891111.
19. Shopera T, Henson WR, Ng A, Lee YJ, Ng K, Moon TS. Robust, tunable genetic memory from protein sequestration combined with positive feedback. Nucleic acids research. 2015;43(18):9086-94. doi: 10.1093/nar/gkv936. PubMed PMID: 26384562; PubMed Central PMCID: PMC4605329.
20. Cheng Z, Liu F, Zhang XP, Wang W. Robustness analysis of cellular memory in an autoactivating positive feedback system. FEBS letters. 2008;582(27):3776-82. doi: 10.1016/j.febslet.2008.10.005. PubMed PMID: 18930050.
21. Kim TH, Jung SH, Cho KH. Interlinked mutual inhibitory positive feedbacks induce robust cellular memory effects. FEBS letters. 2007;581(25):4899-904. doi: 10.1016/j.febslet.2007.09.020. PubMed PMID: 17892872.
22. Acar M, Becskei A, van Oudenaarden A. Enhancement of cellular memory by reducing stochastic transitions. Nature. 2005;435(7039):228-32. doi: 10.1038/nature03524. PubMed PMID: 15889097.
23. Gardner TS, Cantor CR, Collins JJ. Construction of a genetic toggle switch in Escherichia coli. Nature. 2000;403(6767):339-42. doi: 10.1038/35002131. PubMed PMID: 10659857.
24. Frigola D, Casanellas L, Sancho JM, Ibanes M. Asymmetric stochastic switching driven by intrinsic molecular noise. PloS one. 2012;7(2):e31407. doi: 10.1371/journal.pone.0031407. PubMed PMID: 22363638; PubMed Central PMCID: PMC3283640.
25. Cherry JL, Adler FR. How to make a Biological Switch. Journal of theoretical biology. 2000;203(2):117-33. doi: DOI 10.1006/jtbi.2000.1068. PubMed PMID: WOS:000086027600005.
26. Ferrell JE, Xiong W. Bistability in cell signaling: How to make continuous processes discontinuous, and reversible processes irreversible. Chaos. 2001;11(1):227-36. doi: Doi 10.1063/1.1349894. PubMed PMID: WOS:000167301400021.
27. Pedraza JM, Paulsson J. Effects of molecular memory and bursting on fluctuations in gene expression. Science. 2008;319(5861):339-43. doi: 10.1126/science.1144331. PubMed PMID: 18202292.

28. Tabor JJ, Salis HM, Simpson ZB, Chevalier AA, Levskaya A, Marcotte EM, et al. A synthetic genetic edge detection program. Cell. 2009;137(7):1272-81. doi: 10.1016/j.cell.2009.04.048. PubMed PMID: 19563759; PubMed Central PMCID: PMC2775486.
29. Auslander S, Auslander D, Muller M, Wieland M, Fussenegger M. Programmable single-cell mammalian biocomputers. Nature. 2012;487(7405):123-7. doi: 10.1038/nature11149. PubMed PMID: 22722847.
30. Daniel R, Rubens JR, Sarpeshkar R, Lu TK. Synthetic analog computation in living cells. Nature. 2013;497(7451):619-23. doi: 10.1038/nature12148. PubMed PMID: 23676681.
31. Becskei A, Seraphin B, Serrano L. Positive feedback in eukaryotic gene networks: cell differentiation by graded to binary response conversion. The EMBO journal. 2001;20(10):2528-35. doi: 10.1093/emboj/20.10.2528. PubMed PMID: 11350942; PubMed Central PMCID: PMC125456.
32. McAdams HH, Arkin A. Stochastic mechanisms in gene expression. Proceedings of the National Academy of Sciences of the United States of America. 1997;94(3):814-9. doi: DOI 10.1073/pnas.94.3.814. PubMed PMID: WOS:A1997WG23400009.
33. Ozbudak EM, Thattai M, Kurtser I, Grossman AD, van Oudenaarden A. Regulation of noise in the expression of a single gene. Nat Genet. 2002;31(1):69-73. doi: 10.1038/ng869. PubMed PMID: WOS:000175362500017.
34. Sneppen K, Micheelsen MA, Dodd IB. Ultrasensitive gene regulation by positive feedback loops in nucleosome modification. Molecular systems biology. 2008;4:182. doi: 10.1038/msb.2008.21. PubMed PMID: 18414483; PubMed Central PMCID: PMC2387233.
35. Elowitz MB, Levine AJ, Siggia ED, Swain PS. Stochastic gene expression in a single cell. Science. 2002;297(5584):1183-6. doi: 10.1126/science.1070919. PubMed PMID: 12183631.
36. Blake WJ, M KA, Cantor CR, Collins JJ. Noise in eukaryotic gene expression. Nature. 2003;422(6932):633-7. doi: 10.1038/nature01546. PubMed PMID: 12687005.

37. Pedraza JM, van Oudenaarden A. Noise propagation in gene networks. Science. 2005;307(5717):1965-9. doi: 10.1126/science.1109090. PubMed PMID: 15790857.
38. Eldar A, Elowitz MB. Functional roles for noise in genetic circuits. Nature. 2010;467(7312):167-73. doi: 10.1038/nature09326. PubMed PMID: 20829787; PubMed Central PMCID: PMC4100692.
39. Zhang H, Chen Y, Chen Y. Noise propagation in gene regulation networks involving interlinked positive and negative feedback loops. PloS one. 2012;7(12):e51840. doi: 10.1371/journal.pone.0051840. PubMed PMID: 23284787; PubMed Central PMCID: PMC3527455.
40. Tan C, Marguet P, You L. Emergent bistability by a growth-modulating positive feedback circuit. Nature chemical biology. 2009;5(11):842-8. doi: 10.1038/nchembio.218. PubMed PMID: 19801994; PubMed Central PMCID: PMC2908482.
41. Basu S, Gerchman Y, Collins CH, Arnold FH, Weiss R. A synthetic multicellular system for programmed pattern formation. Nature. 2005;434(7037):1130-4. doi: 10.1038/nature03461. PubMed PMID: 15858574.
42. Moon TS, Lou C, Tamsir A, Stanton BC, Voigt CA. Genetic programs constructed from layered logic gates in single cells. Nature. 2012;491(7423):249-53. doi: 10.1038/nature11516. PubMed PMID: 23041931; PubMed Central PMCID: PMC3904217.
43. Kurata H, Maeda K, Onaka T, Takata T. BioFNet: biological functional network database for analysis and synthesis of biological systems. Briefings in bioinformatics. 2014;15(5):699-709. doi: 10.1093/bib/bbt048. PubMed PMID: 23894104.
44. Thomas P, Straube AV, Grima R. Communication: limitations of the stochastic quasi-steady-state approximation in open biochemical reaction networks. The Journal of chemical physics. 2011;135(18):181103. doi: 10.1063/1.3661156. PubMed PMID: 22088045.
45. Hornos JE, Schultz D, Innocentini GC, Wang J, Walczak AM, Onuchic JN, et al. Self-regulating gene: an exact solution. Physical review E, Statistical, nonlinear, and soft matter physics. 2005;72(5 Pt 1):051907. Epub 2005/12/31. doi: 10.1103/PhysRevE.72.051907. PubMed PMID: 16383645.

46. Michael E. Wall. Quantitative Biology: From Molecular to Cellular Systems. Chapman & Hall/CRC Mathematical and Computational Biology. 2012; CRC Press, Boca Raton, Florida.
47. Ul Hasan ABMS, Kurata H. Mathematical comparison of memory functions between mutual activation and repression networks in a stochastic environment. J Theor Biol. 2017;427:28-40. doi: 10.1016/j.jtbi.2017.05.036. PubMed PMID: WOS:000405541200005.
48. Kurata H, Matoba N, Shimizu N. CADLIVE for constructing a large-scale biochemical network based on a simulation-directed notation and its application to yeast cell cycle. Nucleic acids research. 2003;31(14):4071-84. PubMed PMID: 12853624; PubMed Central PMCID: PMC165976.
49. Kurata H, Inoue K, Maeda K, Masaki K, Shimokawa Y, Zhao Q. Extended CADLIVE: a novel graphical notation for design of biochemical network maps and computational pathway analysis. Nucleic acids research. 2007;35(20):e134. doi: 10.1093/nar/gkm769. PubMed PMID: 17940089; PubMed Central PMCID: PMC2175333. 48.
50. Cao Y, Gillespie DT, Petzold LR. Efficient step size selection for the tau-leaping simulation method. The Journal of chemical physics.
51. Matsuda M, Koga M, Woltjen K, Nishida E, Ebisuya M. Synthetic lateral inhibition governs cell-type bifurcation with robust ratios. Nature communications. 2015;6:6195. doi: 10.1038/ncomms7195. PubMed PMID: 25652697.
52. Gillespie DT. Exact Stochastic Simulation of Coupled Chemical-Reactions. J Phys Chem-Us. 1977;81(25):2340-61. doi: Doi 10.1021/J100540a008. PubMed PMID: WOS:A1977EE49800008.
53. Alves R, Savageau MA. Extending the method of mathematically controlled comparison to include numerical comparisons. Bioinformatics. 2000;16(9):786-98. PubMed PMID: 11108701.
54. Scott M, Hwa T, Ingalls B. Deterministic characterization of stochastic genetic circuits. Proceedings of the National Academy of Sciences of the United States of America. 2007;104(18):7402-7. doi: 10.1073/pnas.0610468104. PubMed PMID: WOS:000246239400020.
55. Gillespie DT. The chemical Langevin equation. Journal of Chemical Physics. 2000;113(1):297-306. doi: Pii [S0021-9606(00)50925-8]

56. Gardiner, C.W. Stochastic Methods: A Handbook for the Natural and Social Sciences. Springer Series in Synergetics. 2009; 4th ed. (Springer–Verlag, Berlin).
57. Risken, H., and Frank, T. The Fokker–Planck Equation: Methods of Solution and Applications. 1996; 2nd ed. (Springer, Berlin).
58. Sharma Y, Dutta PS, Gupta AK. Anticipating regime shifts in gene expression: The case of an autoactivating positive feedback loop. Phys Rev E. 2016;93(3):032404. doi: 10.1103/PhysRevE.93.032404. PubMed PMID: 27078387.
59. Drury KLS. Shot noise perturbations and mean first passage times between stable states. Theor Popul Biol. 2007;72(1):153-66. doi: 10.1016/j.tpb.2007.03.010. PubMed PMID: WOS:000248426700014.

Figures

Legends

Fig 1. Schematics of two mutual repression network models.

(A) Wiring diagram of the mutual repression network (MRN) model. The protein $y(1)$ acts as a switch for mutual repression network consisting of $y(2)$and $y(3)$. (B) Wiring diagram of the mutual repression network with negative autoregulation (MRN-NA) model. The added negative autoregulation reactions that regulate he protein synthesis of $y(2)$ and $y(3)$ are highlighted in red. All reaction rates k and dissociation constants K are listed in Tables 1 and 2.

Fig 2. Deterministic and stochastic simulations of the MRN model

(A) Deterministic simulation of proteins $y(1)$, $y(2)$ and $y(3)$ at different Hill coefficients. The input signal S is applied from time steps 250 to 500. The dissociation constants are set to $K(2) = K(4) = 43$; all other corresponding parameter values are listed in Table 3. The simulated time evolution is shown for $y(2)$ and $y(3)$ at $n = 7$ (red and magenta lines), and $n = 8$ (black and cyan lines).

(B) The hysteresis curves of $y(2)$ at different Hill coefficients $n = 7$ and $n = 8$ are consistent with the deterministic simulations (C) The hysteresis curves of $y(3)$ at different Hill coefficients $n = 7$ and $n = 8$ are consistent with the deterministic simulations. (D) Trajectories of the stochastic simulation of $y(1)$, $y(2)$ and $y(3)$ at Hill coefficient $n = 7$. (E) Trajectories of the stochastic simulation of $y(1)$, $y(2)$ and $y(3)$ at Hill coefficient $n = 8$.

Fig 3. Deterministic and stochastic simulations of the MRN-NA model

(A) Deterministic simulation of proteins $y(1)$, $y(2)$ and $y(3)$ at different Hill coefficients. The input signal S is applied from time steps 250 to 500. The dissociation constants are set to $K(2) = K(4) = 43$; all other corresponding parameter values are set as the same as the MRN model (Table 3). The simulated time evolution is shown for $y(2)$ and $y(3)$ at $n = 7$ (red and magenta lines), and at $n = 8$ (black and

cyan lines). (B) The hysteresis curves of $y(2)$ at different Hill coefficients $n = 7$ and $n = 8$ are consistent with the deterministic simulations (C) The hysteresis curves of $y(3)$ at different Hill coefficients $n = 7$ and $n = 8$ are consistent with the deterministic simulations. (D) Trajectories of the stochastic simulation of $y(1)$, $y(2)$ and $y(3)$ at Hill coefficient $n = 7$. (E) Trajectories of the stochastic simulation of $y(1)$, $y(2)$ and $y(3)$ at Hill coefficient $n = 8$. (F) Stochastic fluctuations in the MRN and MRN-NA models. The coefficients of variation (CVs) are computed from the simulated stochastic trajectories during the signal period as function of changing dissociation constants $K(2) = K(4)$. More optimal comparability between the two models, the parameters associated to the negative autoregulation reactions were tuned to conserve the steady state levels between both models. Shown are the CVs of $y(2)$ (MRN: red line; MRN-NA: black line), and $y(3)$ (MRN: magenta line; MRN-NA: cyan line).

Fig 4. Phase diagram of the memory regions for the MRN and the MRN-NA models

(A) The memory region of the MRN model. (B) The memory region of the MRN-NA model. The memory regions are illustrated with respect to the Hill coefficient and dissociation constants. The deterministic memory region is defined by the region that includes both the cyan and red areas, whereas the stochastic memory regions are shown in red.

Fig. 5 Phase diagram of the stochastic bistable regions for the MRN and the MRN-NA models

Phase diagrams of the stochastic bistable regions as function of Hill coefficient and dissociation constant in the mutual repression cycle for $y(2)$ in the MRN (A) and MRN-NA (B), and for $y(3)$ in the MRN (C) and MRN-NA (D) models.

Fig. 6 Mean first passage time (MFPT) analysis of the MRN and the MRN-NA

(A) The logarithmic MFPTs of the low and high steady states of $y(2)$ ($T_L(y(2)_l^{st})$ and $T_U(y(2)_u^{st})$) and $y(3)$ ($T_L(y(3)_l^{st})$ and $T_U(y(3)_u^{st})$) are shown for the MRN and MRN-NA models as function of the Hill coefficient.

(B) The logarithmic MFPTs of the low and high steady states of $y(2)$ and $y(3)$ denoted as above are shown for the MRN and MRN-NA as function of the dissociation constant .

Fig. 7 Probability density of the steady-state levels in the MRN and the MRN-NA

Probability densities computed from the Fokker-Planck equations of the MRN and MRN-NA models. (A) Probability density of $y(2)$ in the MRN and the MRN-NA as function of the Hill coefficient. (B) Probability density of $y(3)$ in the MRN and the MRN-NA as function of the Hill coefficient. (C) Probability density of $y(2)$ in the MRN and the MRN-NA as function of the dissociation constant. (D) Probability density of $y(3)$ in the MRN and the MRN-NA as function of the dissociation constant.

Tables

Table 1. List of kinetic parameters used in the two gene regulatory networks

Kinetic parameters	**Definition**
$k(1)$, $k(3)$, $k(4)$, $k(6)$, $k(7)$	protein synthesis rate constants
$k(2)$, $k(5)$, $k(8)$	degradation rate constants
$K(1)$, $K(2)$, $K(3)$, $K(4)$	dissociation constants of activators / repressor
$k(9)$, $k(10)$	protein synthesis rate constants of negative autoregulation
$K(5)$, $K(6)$	dissociation constants of negative autoregulation
n	Hill coefficient

Table 2. The levels of the gene expression of the MRN and the MRN-NA models at the steady state

	MRN	MRN-NA
Conserved function within each network	The high steady-state level of $y(2)$ and $y(3)$	The high steady-state level of $y(2)$ and $y(3)$
Conserved function MRN and MRN-NA models	The high steady-state level of $y(2)$ and $y(3)$, The low steady-state can be kept at the same level among the two networks as much as possible.	

Table 3. Settings of the corresponding kinetic parameters for the two models

	MRN	MRN-NA
Corresponding parameters within each network	$k(3)=k(6)=18.1$ $k(4)>k(7),\ \ k(7)=43.1$ $k(5)=k(8)=0.8$ $K(1)=K(3)=9$ $K(2)=K(4)=43$ $n=8$	$k(3)=k(6)=18.1$ $k(4)>k(7),\ \ k(7)=43.1$ $k(5)=k(8)=0.8$ $K(1)=K(3)=9$ $K(2)=K(4)=43$ $n=8$ $k(9)=k(10)=4.1$ $K(5)=K(6)=9$
Corresponding parameters and MRN and MRN-NA models	$k(1)\ k(2)\ k(3)\ k(4)\ k(5)\ k(6)\ k(7)\ k(8)$ $K(1)\ K(2)\ K(3)\ K(4)$	

Figure 1

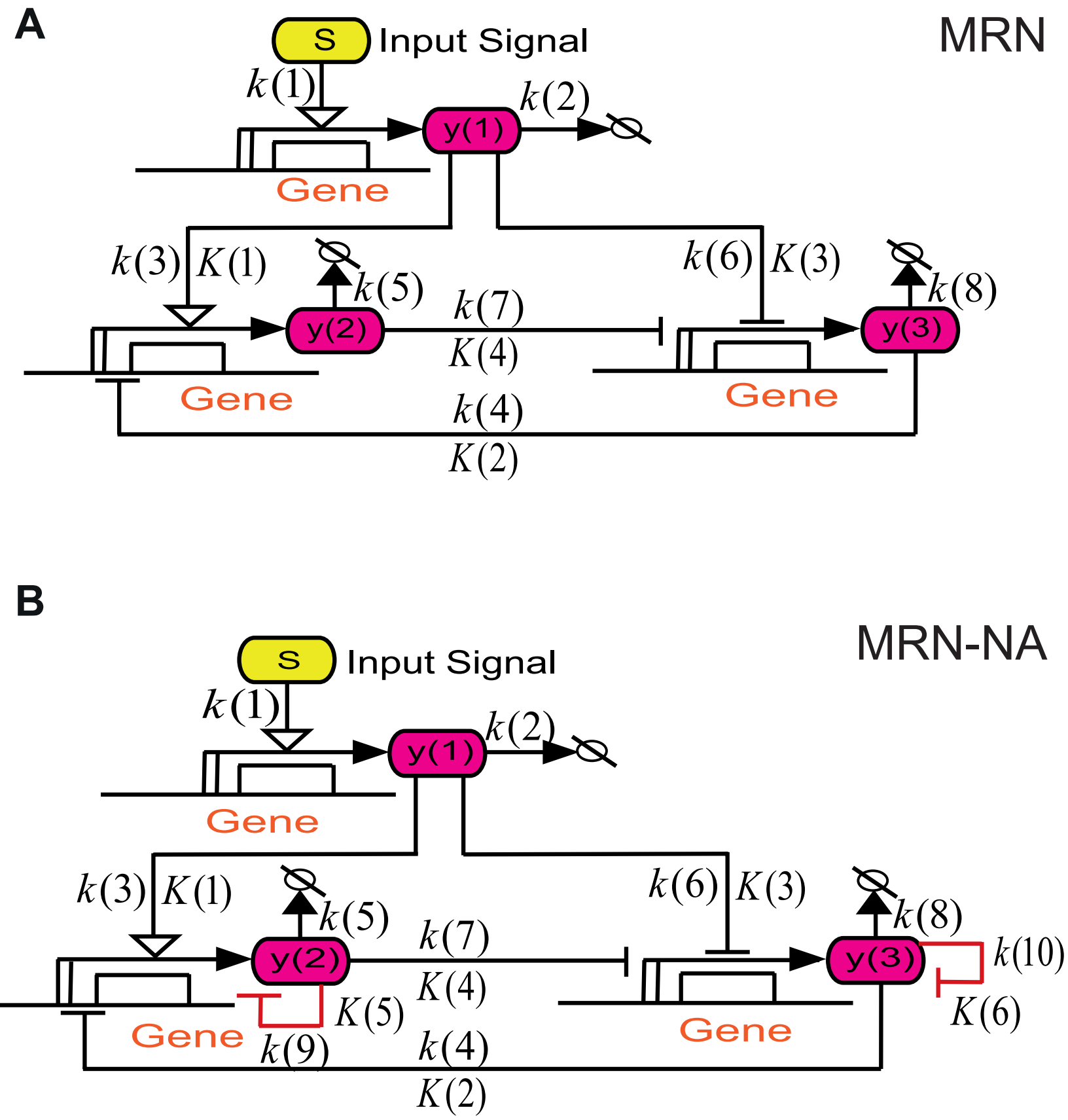
A
MRN
S
Input Signal
k(1)
k(2)
y(1)
Gene
k(3)
K(1)
k(5)
k(7)
K(4)
y(2)
k(6)
K(3)
k(8)
y(3)
Gene
Gene
k(4)
K(2)
B
MRN-NA
S
Input Signal
k(1)
k(2)
y(1)
Gene
k(3)
K(1)
k(5)
k(7)
K(4)
y(2)
K(5)
k(9)
Gene
k(6)
K(3)
k(8)
y(3)
k(10)
K(6)
Gene
k(4)
K(2)

Figure 2

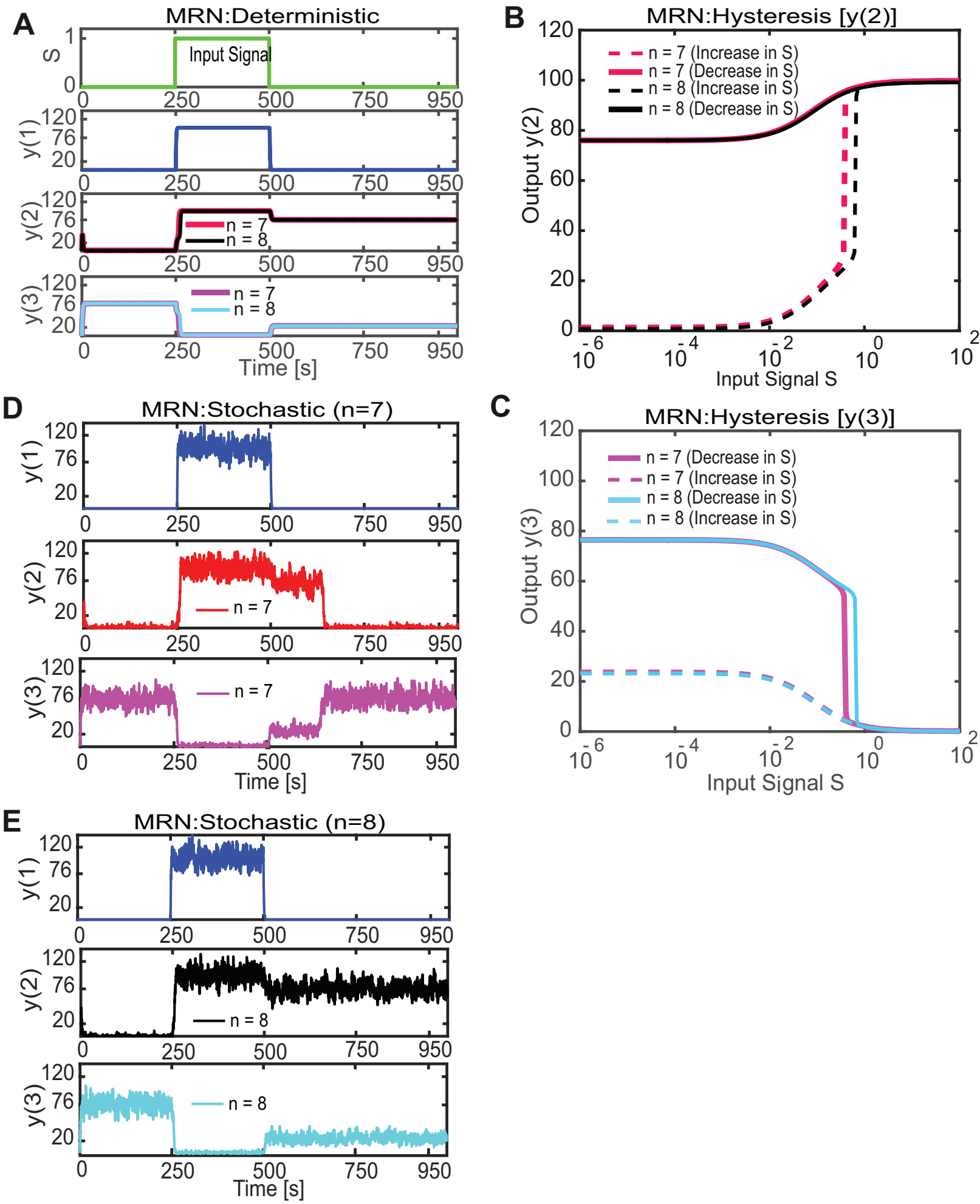
A
MRN:Deterministic
S
Input Signal
y(1)
y(2)
y(3)
n = 7
n = 8
Time [s]
B
MRN:Hysteresis [y(2)]
n = 7 (Increase in S)
n = 7 (Decrease in S)
n = 8 (Increase in S)
n = 8 (Decrease in S)
Output y(2)
Input Signal S
C
MRN:Hysteresis [y(3)]
n = 7 (Decrease in S)
n = 7 (Increase in S)
n = 8 (Decrease in S)
n = 8 (Increase in S)
Output y(3)
Input Signal S
D
MRN:Stochastic (n=7)
E
MRN:Stochastic (n=8)

Figure 3

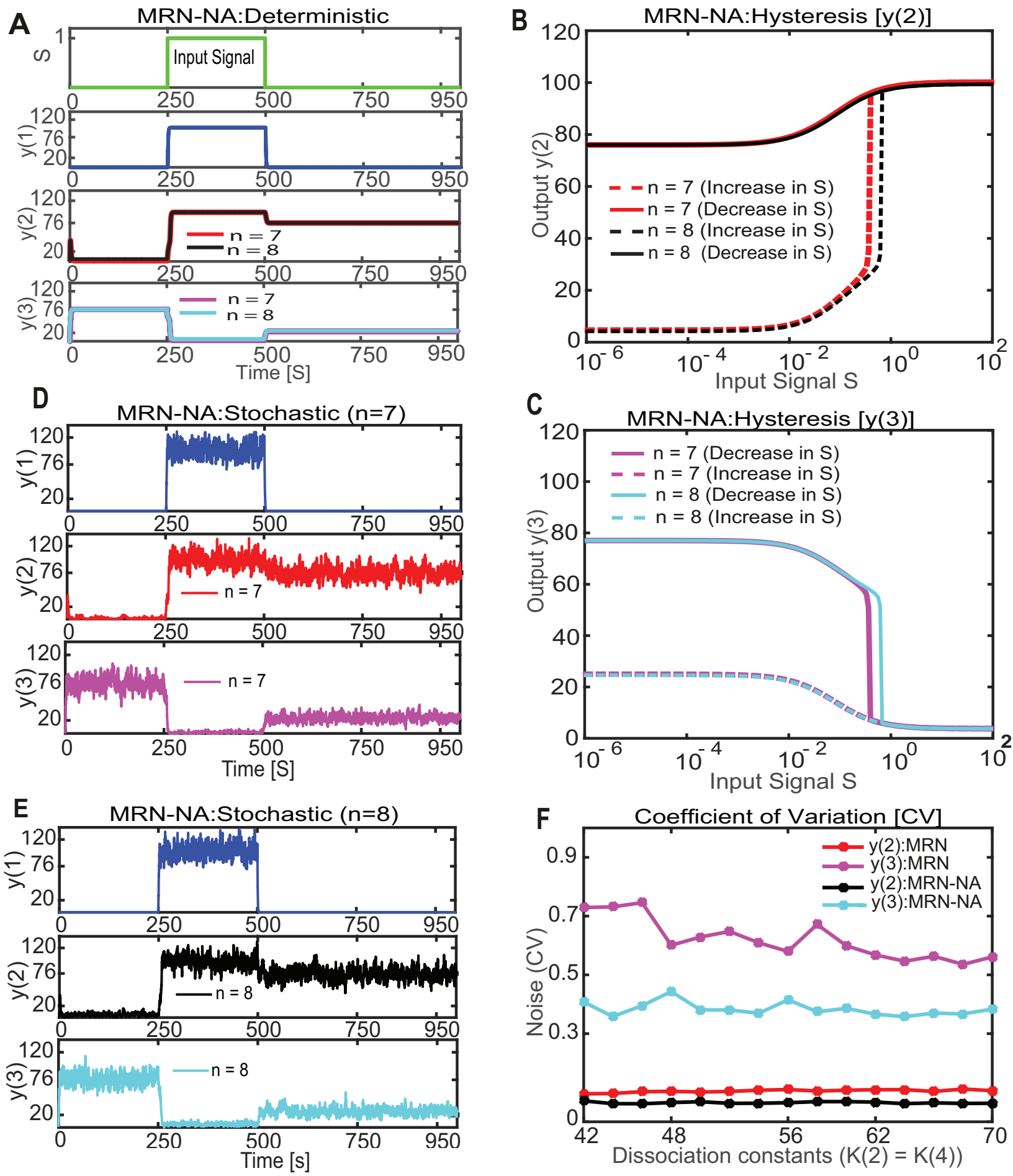
A
MRN-NA:Deterministic
S
Input Signal
y(1)
y(2)
y(3)
n = 7
n = 8
Time [S]
B
MRN-NA:Hysteresis [y(2)]
Output y(2)
n = 7 (Increase in S)
n = 7 (Decrease in S)
n = 8 (Increase in S)
n = 8 (Decrease in S)
Input Signal S
D
MRN-NA:Stochastic (n=7)
Time [S]
C
MRN-NA:Hysteresis [y(3)]
Output y(3)
n = 7 (Decrease in S)
n = 7 (Increase in S)
n = 8 (Decrease in S)
n = 8 (Increase in S)
Input Signal S
E
MRN-NA:Stochastic (n=8)
Time [s]
F
Coefficient of Variation [CV]
y(2):MRN
y(3):MRN
y(2):MRN-NA
y(3):MRN-NA
Noise (CV)
Dissociation constants (K(2) = K(4))

Figure 4

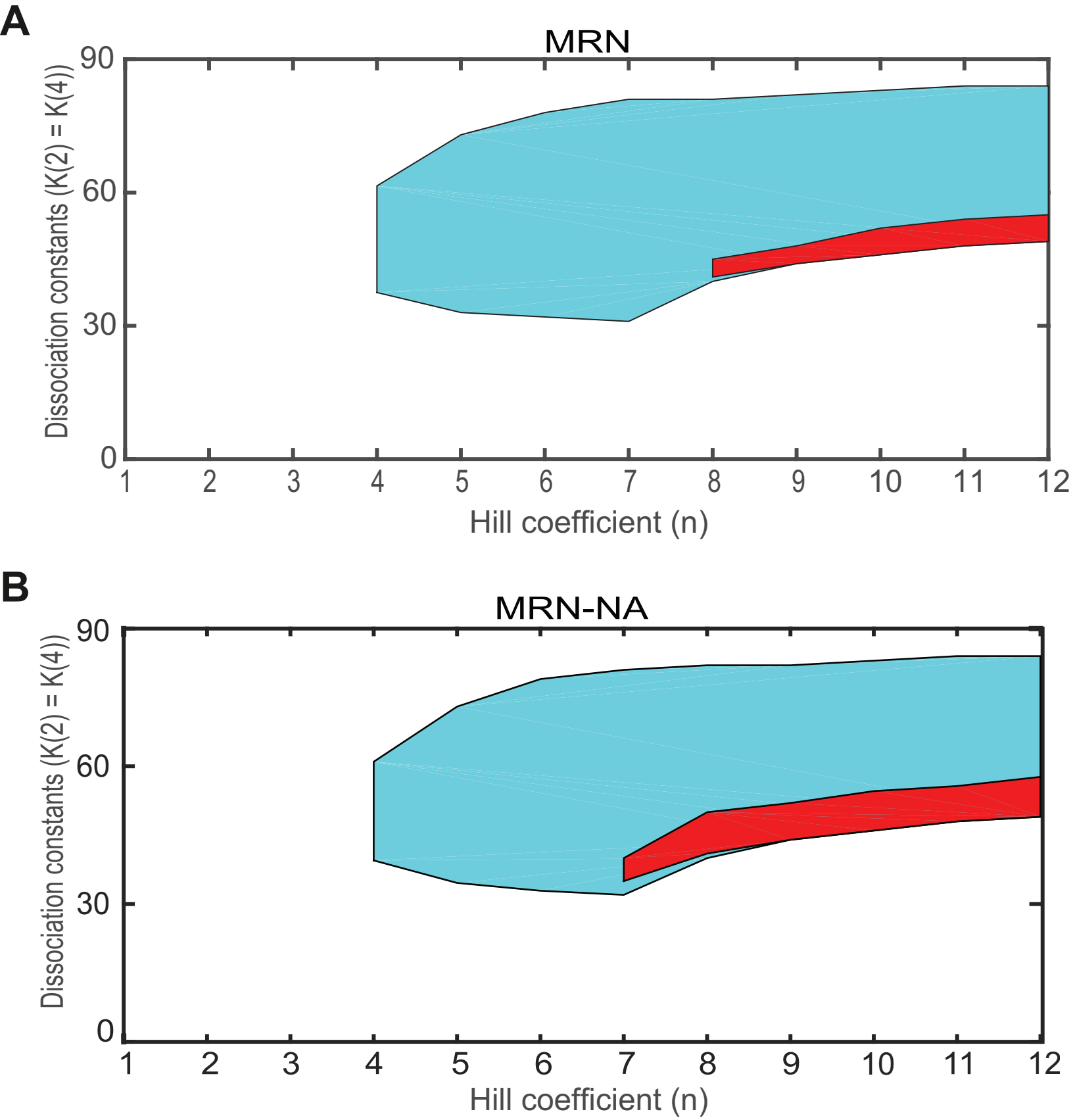
A
MRN
Dissociation constants (K(2) = K(4))
90
60
30
0
1
2
3
4
5
6
7
8
9
10
11
12
Hill coefficient (n)
B
MRN-NA
Dissociation constants (K(2) = K(4))
90
60
30
0
1
2
3
4
5
6
7
8
9
10
11
12
Hill coefficient (n)

Figure 5

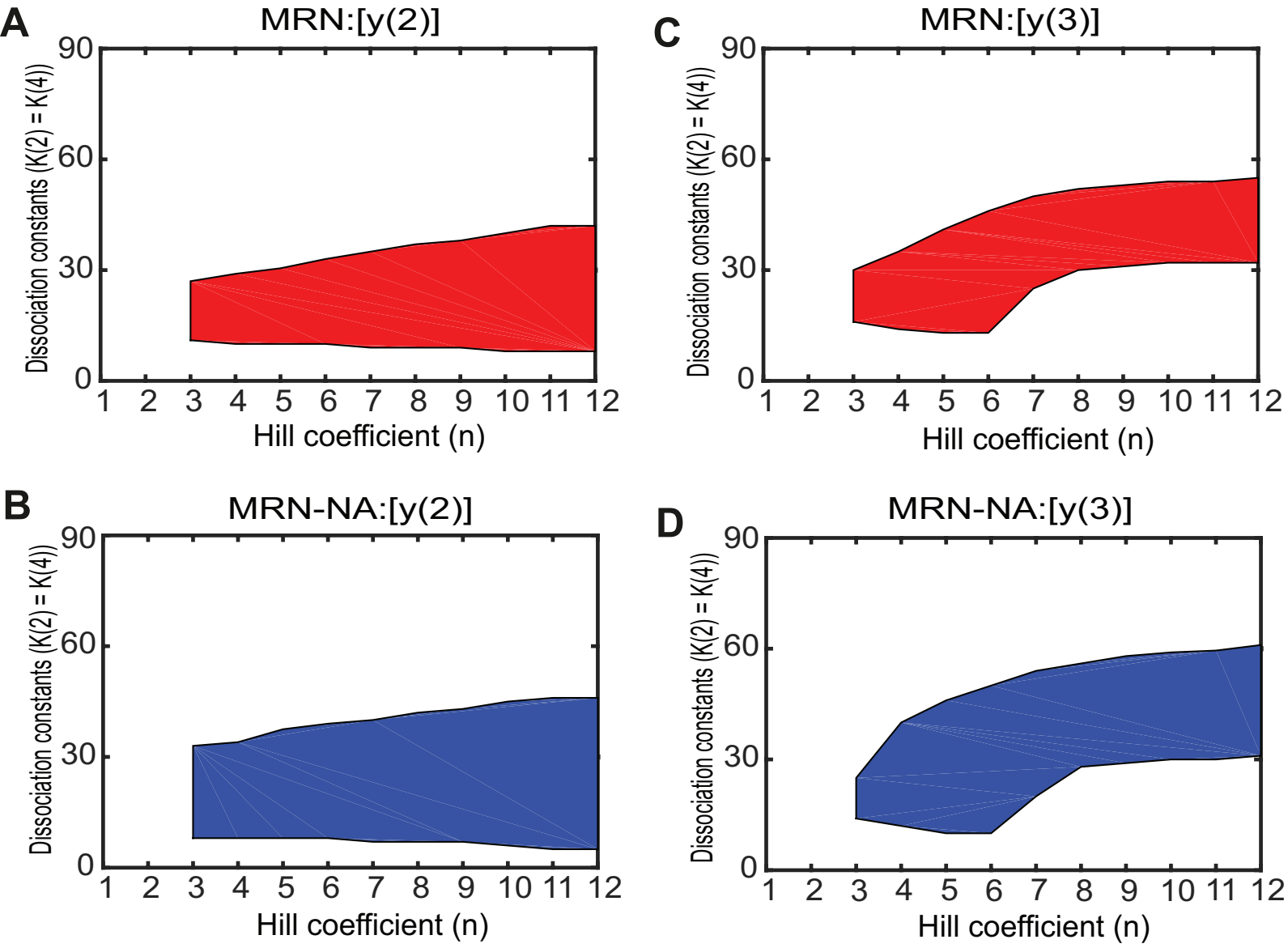
A
MRN:[y(2)]
B
MRN-NA:[y(2)]
C
MRN:[y(3)]
D
MRN-NA:[y(3)]
Dissociation constants (K(2) = K(4))
Hill coefficient (n)
0
30
60
90
1 2 3 4 5 6 7 8 9 10 11 12

Figure 6

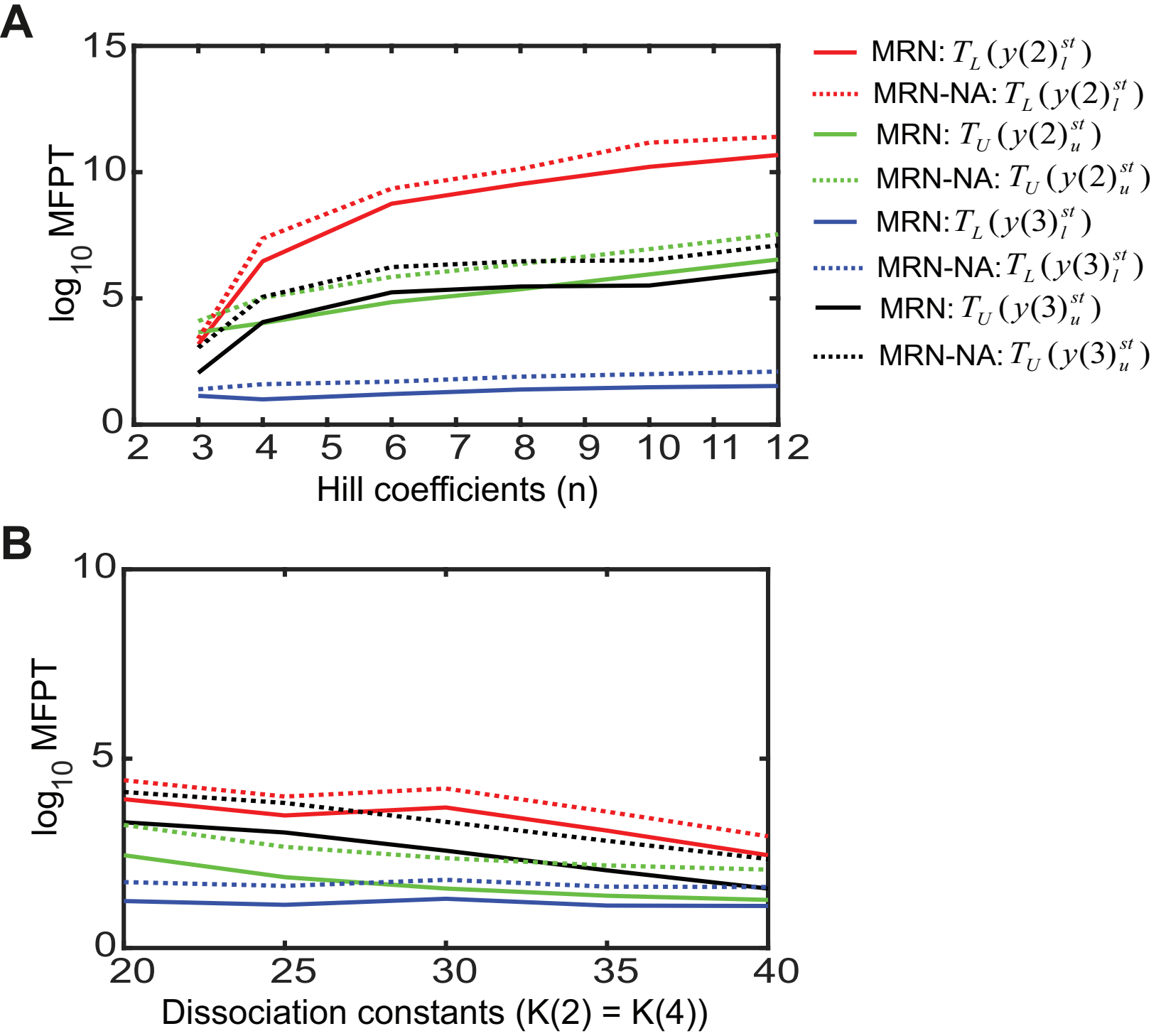
A
15
10
5
0
log10 MFPT
2 3 4 5 6 7 8 9 10 11 12
Hill coefficients (n)
MRN: $T_L(y(2)_l^{st})$
MRN-NA: $T_L(y(2)_l^{st})$
MRN: $T_U(y(2)_u^{st})$
MRN-NA: $T_U(y(2)_u^{st})$
MRN: $T_L(y(3)_l^{st})$
MRN-NA: $T_L(y(3)_l^{st})$
MRN: $T_U(y(3)_u^{st})$
MRN-NA: $T_U(y(3)_u^{st})$
B
10
5
0
log10 MFPT
20 25 30 35 40
Dissociation constants (K(2) = K(4))

Figure 7

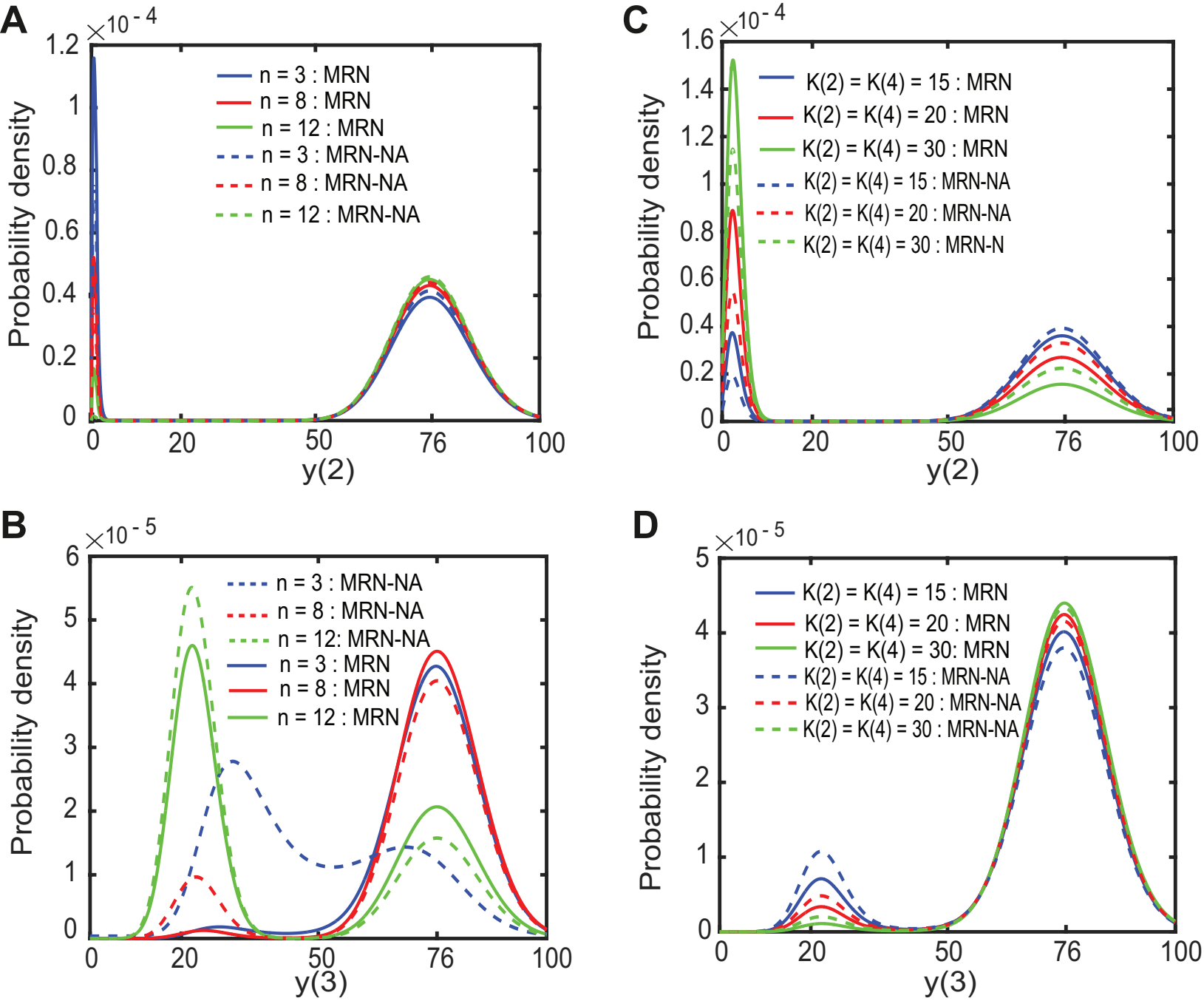
A
×10 - 4
Probability density
y(2)
n = 3 : MRN
n = 8 : MRN
n = 12 : MRN
n = 3 : MRN-NA
n = 8 : MRN-NA
n = 12 : MRN-NA
B
×10 - 5
Probability density
y(3)
n = 3 : MRN-NA
n = 8 : MRN-NA
n = 12: MRN-NA
n = 3 : MRN
n = 8 : MRN
n = 12 : MRN
C
×10 - 4
Probability density
y(2)
K(2) = K(4) = 15 : MRN
K(2) = K(4) = 20 : MRN
K(2) = K(4) = 30 : MRN
K(2) = K(4) = 15 : MRN-NA
K(2) = K(4) = 20 : MRN-NA
K(2) = K(4) = 30 : MRN-N
D
×10 - 5
Probability density
y(3)
K(2) = K(4) = 15 : MRN
K(2) = K(4) = 20 : MRN
K(2) = K(4) = 30: MRN
K(2) = K(4) = 15 : MRN-NA
K(2) = K(4) = 20 : MRN-NA
K(2) = K(4) = 30 : MRN-NA

Figure S1

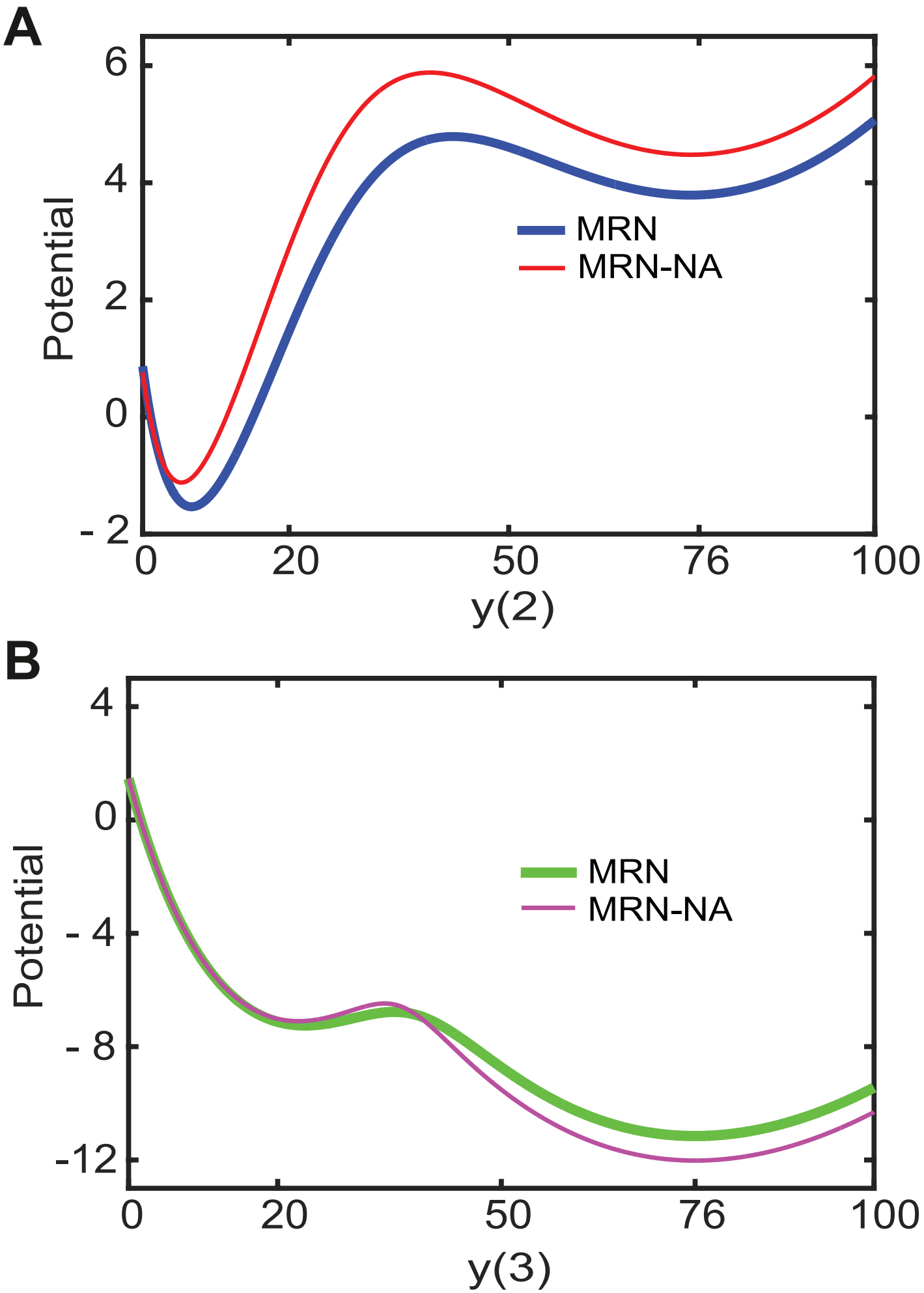
A
6
4
2
0
- 2
Potential
MRN
MRN-NA
0
20
50
76
100
y(2)
B
4
0
- 4
- 8
-12
Potential
MRN
MRN-NA
0
20
50
76
100
y(3)

Figure S2

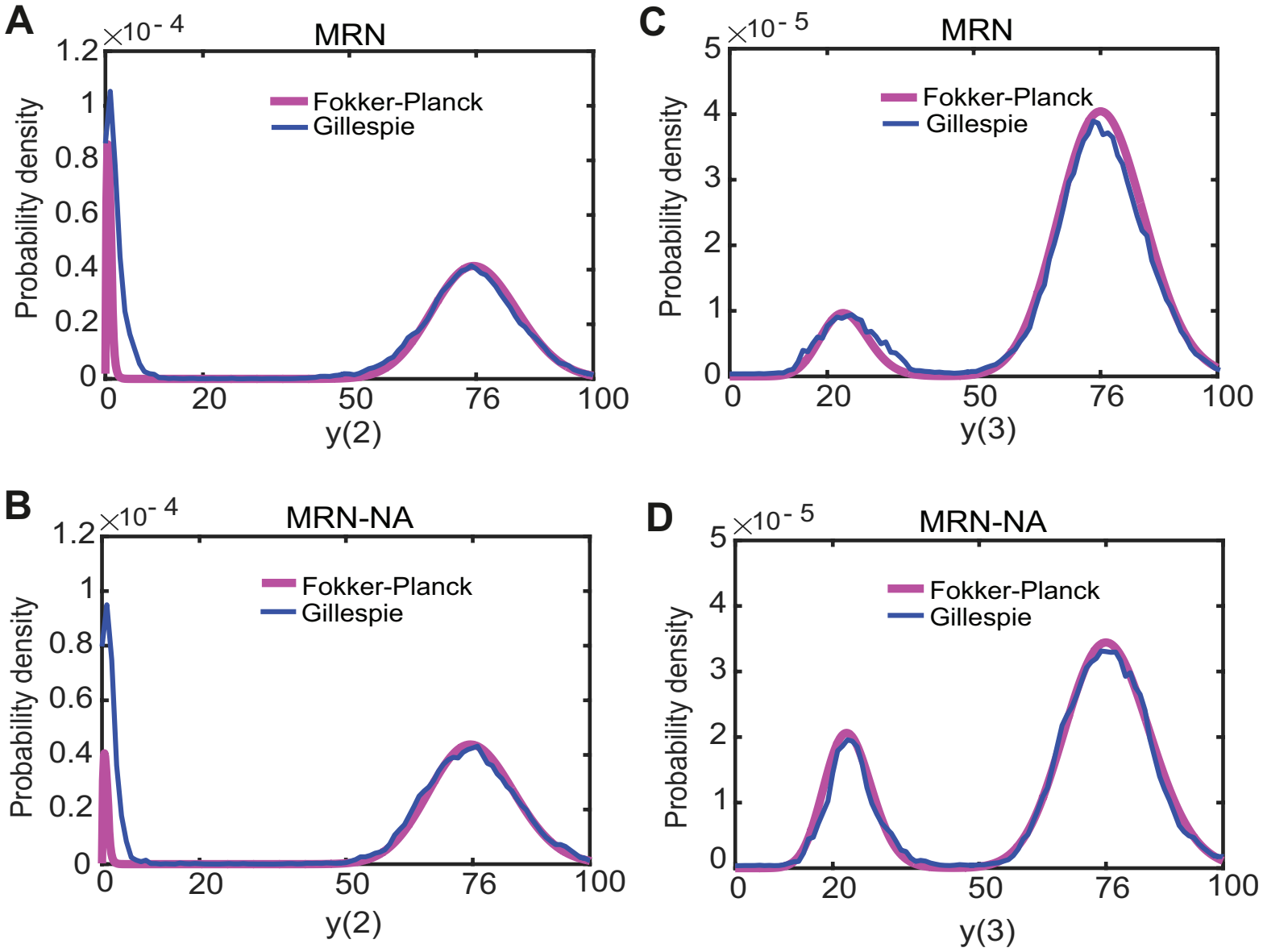
A
MRN
×10⁻⁴
1.2
1
0.8
0.6
0.4
0.2
0
Probability density
Fokker-Planck
Gillespie
0
20
50
76
100
y(2)
C
MRN
×10⁻⁵
5
4
3
2
1
0
Probability density
Fokker-Planck
Gillespie
0
20
50
76
100
y(3)
B
MRN-NA
×10⁻⁴
1.2
1
0.8
0.6
0.4
0.2
0
Probability density
Fokker-Planck
Gillespie
0
20
50
76
100
y(2)
D
MRN-NA
×10⁻⁵
5
4
3
2
1
0
Probability density
Fokker-Planck
Gillespie
0
20
50
76
100
y(3)